SENSITIVITY OF THE BEHAVIOR OF BACKFLOW CEX IONS TO ION ENGINE PLUME CHARACTERISTICS

M. Matsushiro,* M. Nishida,* H. Kuninaka,† K. Toki†

*Department of Aeronautics and Astronautics, Kyushu University
Fukuoka 812-8581, Japan

†Institute of Space and Astronautical Science
Sagamihara, Kanagawa 229-8510, Japan

Abstract

A plume from the MUSES-C ion engine was numerically analyzed using the DSMC-PIC method. Computed results were compared with experimental ones, and the optimal parameters were sought so as to fit to the experiments. Thus determined optimal parameters are the beam expansion angle of 15° and the Gaussian density profile coefficient of 0.6. In the second stage, the sensitivities of the behavior of CEX ion in the backflow region to charge-exchange cross section, electron temperature, Gaussian density profile coefficient and beam expansion angle were investigated. Finally, the effect of the back wall on the behavior of CEX ion flux was examined.

1 Introduction

Xe is widely used as propellant of ion engines. Xe ions are electrostatically accelerated into space as a very fast ion beam. On the other hand, non-ionized Xe atoms (neutrals) are discharged from the ion engine at their sound velocity. These slow neutrals may collide with very rapid ions and as a result some of these collisions lead to CEX reaction (Charge Exchange Reaction) as shown below.

$$\mathrm{Xe}^{+}_{\mathrm{fast}} + \mathrm{Xe}_{\mathrm{slow}} \longrightarrow \mathrm{Xe}^{+}_{\mathrm{slow}} + \mathrm{Xe}_{\mathrm{fast}} \tag{1}$$

This process generates highly energetic neutrals and slow ions (CEX ions). The slow ions are scattered away from the ion beam and may interact with the spacecraft surface, whereby the surface material properties may be altered. Therefore, it is important to estimate the amount of the CEX ion in the backflow region.

The present paper concerns numerical analysis of an ion engine plume and backflow CEX ions. The numerical method used here is the combination of the Direct Simulation Monte Carlo (DSMC) method [1][2] and particle-in-cell (PIC) method [3][4]. The DSMC method is used to deal with collisions of neutral particles and the PIC method is used to determine the trajectories of charged particles. The numerical code was tested on the ion engine of the MUSES-C (Table 1) prepared at the Institute of Space and Astronautical Science (ISAS), and computed results were compared with experimental results. It is the main objective to investigate the behavior of backflow CEX ions and to reveal the sensitivity of them to ion engine plume characteristics.

Several numerical studies of a plume discharged from an ion thruster have been conducted [5]-[11]. Wang et al. carried out 3-D simulations of the ion thruster by using the PIC-MCC model [5], [6]. Samanta Roy et al. investigated the structure of ion thruster plume and the backflow applying the PIC technique to charged particles [7]-[9]. In these studies, a single-point source flow was assumed to model the neutral density field. On the other hand, VanGilder et al. simultaneously treated both neutral atoms and ions as particles by using the hybrid DSMC-PIC code, and revealed the ion beam characteristics of an ion thruster [11]. They found from the comparisons of computed results of axial and radial profiles of beam ion flux with existing experimental ones that the beam ions are only moderately dependent on the cross section for charge-exchange reactions, the mechanics of charge exchange reactions and the electron temperature, and that CEX ions are sensitive to them.

Table 1. MUSES-C ion engine.

Mass flow rate	Beam voltage	Beam current	Thruster exit radius
0.21 mg/s	1,500 V	0.14 A	105 mm

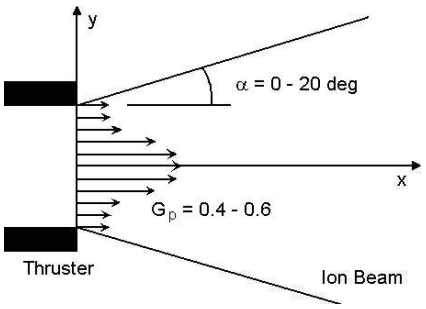

Figure 1. Gaussian distribution and beam angle of an ion beam.

2 Numerical Method

The PIC method determines the trajectory of an ion, for which electric filed is needed, and the electric field can be derived from electric potential. Therefore, our problem is how to determine the potential. In an ion engine, beam ions are neutralized outside the thruster by electrons emitted from neutralizers. In this paper, it is assumed that electrons neutralize Xe ions in the plume, which leads to a quasi-neutral state ($n_{\rm i}{\approx}n_{\rm e}$). These electrons are considered to obey a Boltzmann distribution: [7]

$$n_{\rm e} = n_{\rm ref} \exp(e\phi/kT_{\rm e}) \tag{2}$$

where $n_{\rm e}$ is the electron number density, $n_{\rm ref}$ is the electron number density at reference point ($\phi = 0$), e is the electronic charge, ϕ is the potential, k is the Boltzmann constant and $T_{\rm e}$ is the electron temperature. The electron temperature is treated as one of parameters in this calculation. Once ion density is determined, the electric potential can be obtained by Eq. (2).

Collisions between neutrals are elastic, and the momentum is transferred between them. The scattering angle is chosen randomly from an isotropic distribution and the variable hard-sphere (VHS) model is used for these collisions. Collisions between neutrals and ions, which is the charge-exchange reaction, generate CEX ions. The probability of the charge-exchange reaction is based on the relative velocity through the collision cross section and is given by Rapp and Francis [12]. The production rate of CEX ion $\dot{n}_{\rm cex}$ is given by

$$\dot{n}_{\rm cex} = n_{\rm n} n_{\rm bi} v_{\rm bi} \sigma_{\rm cex}(v_{\rm bi}) \tag{3}$$

where $n_{\rm n}$ is the Xe neutral number density, $n_{\rm bi}$ is the beam ion number density, $v_{\rm bi}$ is the relative velocity between a neutral and a beam ion, and $\sigma_{\rm cex}$ is the collision cross section for the CEX reaction. Pollard [13] suggested that the charge-exchange cross section for Xe is 3 to 8 times higher than that given by Rapp and Francis [12]. Therefore, the charge-exchange cross section is taken to be one of the parameters in this study.

The velocity of Xe neutrals at the thruster exit is assumed to be sonic at 500 K. A radial profile of ion number density at the thruster exit is expressed by a Gaussian density profile:

$$\frac{r}{R} = G_{\rm p} \sqrt{\left| \ln \frac{n_{\rm bi}}{n_{\rm o}} \right|} \tag{4}$$

where $G_{\rm p}$ is the Gaussian ion density profile coefficient, r is the radial coordinate, R is the radius of the thruster exit, $n_{\rm bi}$ is the beam ion number density at r and $n_{\rm o}$ is the ion number density at the center of the thruster exit. It was reported that an actual radial profile of ion number density was sharper than the Gaussian density profile [14], so that the Gaussian density profile coefficient $G_{\rm p}$ was introduced to express such a sharp profile as shown in Fig. 1. The expansion angle of the ion beam is

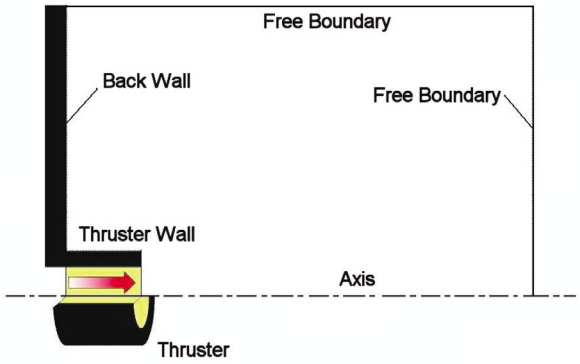

Figure 2. Computational domain and boundary condition without back wall.

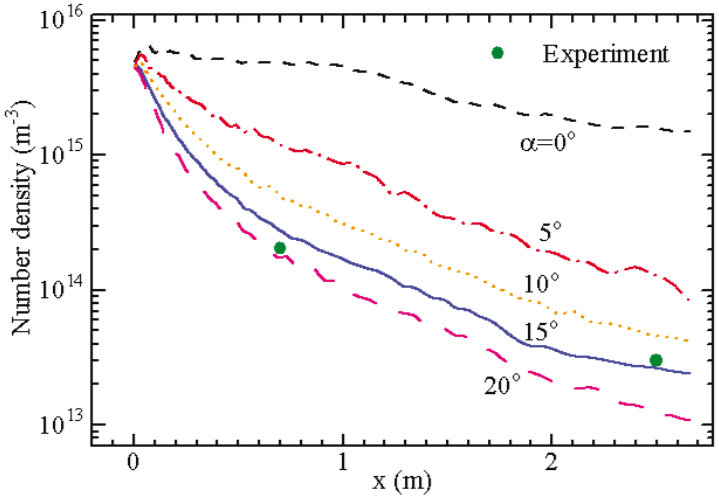

Figure 3. On-axis profiles of ion number density. $\sigma = \sigma_{\rm cex}$, $T_{\rm e} = 1$ eV

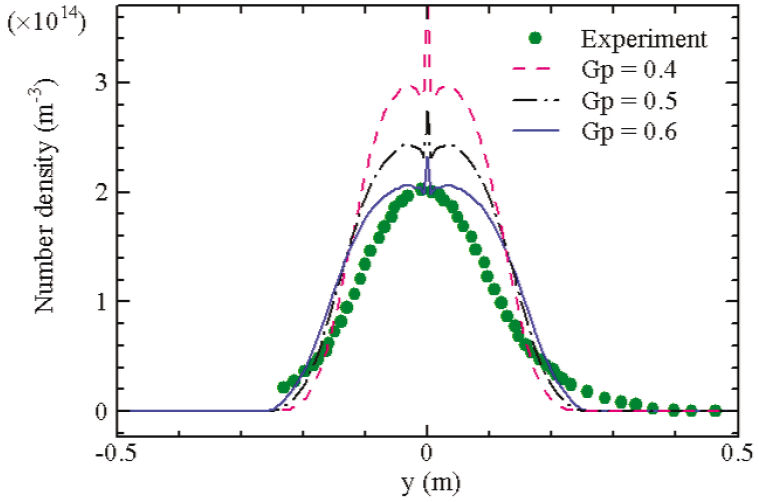

Figure 4. Radial profiles of ion number density at $x = 0.7$ m. $\sigma = \sigma_{\rm cex}$, $T_{\rm e} = 1$ eV

also treated as one of the parameters. Thus, four parameters treated here are charge-exchange cross section ($\sigma_{\rm cex}$), electron temperature ($T_{\rm e}$), Gaussian density profile coefficient ($G_{\rm p}$) and beam expansion angle (α).

Boundary conditions used in the simulation are shown in Fig. 2. The computational domain is axisymmetric, composed of approximately 6,000 cells, and the number of sample particles is about 10^5 to 10^6. Diffuse reflection is imposed at the thruster wall and the back wall. Particles that reach

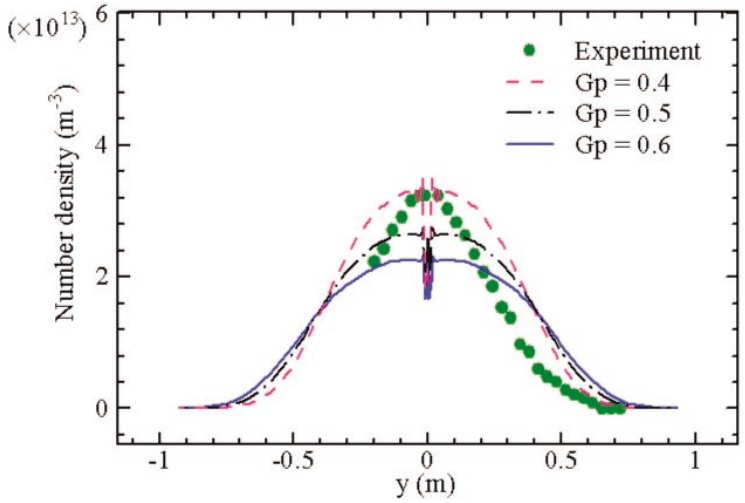

Figure 5. Radial profiles of ion number density at $x = 2.5$ m. $\sigma = \sigma_{\rm cex}$, $T_{\rm e} = 1$ eV

boundaries other than the symmetry line leave the simulation.

Of four parameters, the beam expansion angle and Gaussian density profile coefficient are determined by the comparison of computations with experiments. In addition, sensitivities of the CEX ion current flux in the backflow region to the four parameters are investigated, and furthermore the effect of back wall on the behavior of CEX ions is examined.

3 Results and Discussion

3.1 Ion Density in a Plume

Beam ion number densities computed for ion beam expansion angles of 0° to 20° and Gaussian density profile coefficients of 0.4 to 0.6 were compared with experimental results [15], and then these two parameters were determined so as to satisfy the experimental results. In the computations, the charge-exchange cross section given by Rapp and Francis was used and electron temperature was set to 1 eV in the entire flowfield.

The ion number density along the centerline (x-axis) is shown in Fig. 3 and compared with the experiments. It is seen that the ion number density is decreased as the beam angle is increased. Although there are only two experimental points on this figure, they look to satisfy the profile for the beam expansion angle $\alpha = 15°$. Hence this value may be adopted as a beam expansion angle.

Radial profiles at $x = 0.7$ m and 2.5 m are shown in Figs. 4 and 5. It can be seen that the computed result for the Gaussian density profile coefficient ($G_{\rm p}$) of 0.6 is close to the experimental one. However, the Gaussian density profile coefficient that shows a satisfactory agreement between the computation and experiment in Fig. 5 is 0.4. CEX ions are generated mainly around the thruster exit, where number densities of both neutrals and ions are the largest. The main purpose of this paper is to investigate the behavior of CEX ions in the backflow region, and it is reasonable to adopt $G_{\rm p} = 0.6$ that gives satisfactory agreement between the computation and experiment at the position nearer the thruster exit. Therefore, hereafter $G_{\rm p} = 0.6$ is used for all the computations.

3.2 Analysis of Backflow without Back Wall

Sensitivities of the behavior of CEX ions in the backflow region to charge-exchange cross section, electron temperature, Gaussian density profile coefficient and beam expansion angle were investigated, setting one of these four parameters as variable and keeping the other three parameters as constant. The constant values are such that the charge-exchange cross section $\sigma_{\rm cex}$ is the original value given by Rapp and Francis [12], the electron temperature is 1 eV, Gaussian density profile coefficient is 0.6 and beam angle is 15°. As aforementioned, the latter two values were determined from fitting computed ion number density to the experimental results.

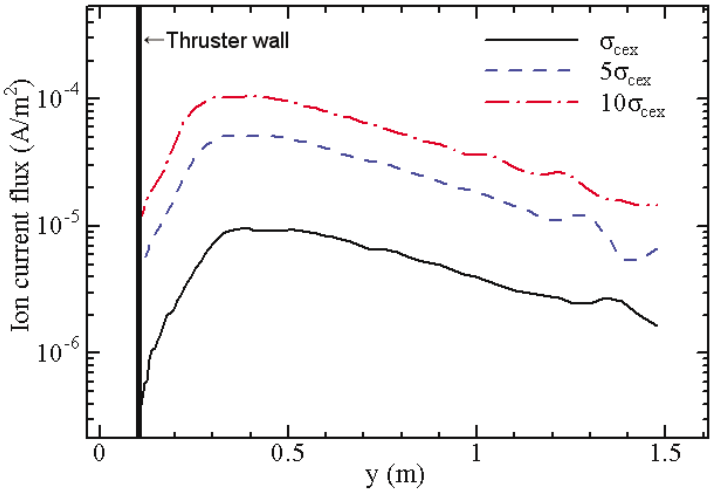

Figure 6. Sensitivity of radial profile of ion current flux to cross section for charge exchange reaction σ_{cex} at x = -0.2 m. $\sigma = \sigma_{\mathrm{cex}}$, $G_{\mathrm{p}} = 0.6$, $\alpha = 15°$.

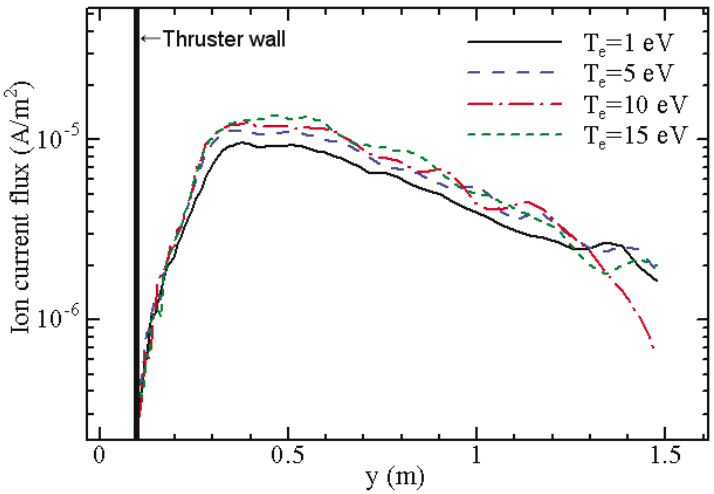

Figure 7. Sensitivity of radial profile of ion current flux to electron temperature T_{e} at x = -0.2 m. $\sigma = \sigma_{\mathrm{cex}}$, $G_{\mathrm{p}} = 0.6$, $\alpha = 15°$.

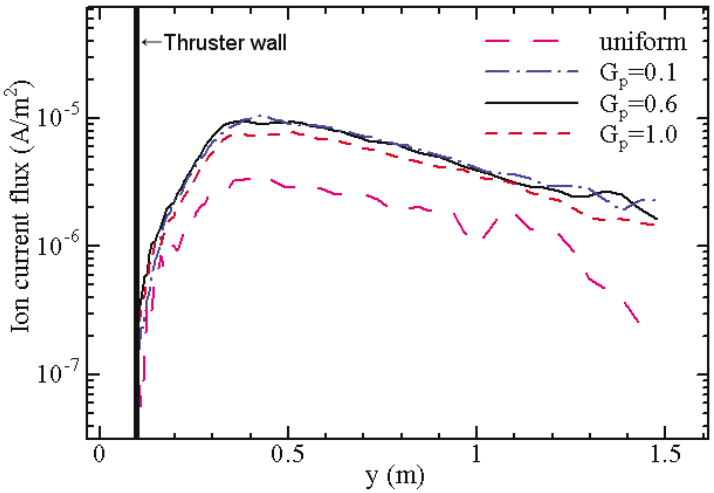

Figure 8. Sensitivity of radial profile of ion current flux to Gaussian density profile coefficient G_{p} at x = -0.2 m. $\sigma = \sigma_{\mathrm{cex}}$, $G_{\mathrm{p}} = 0.6$, $\alpha = 15°$.

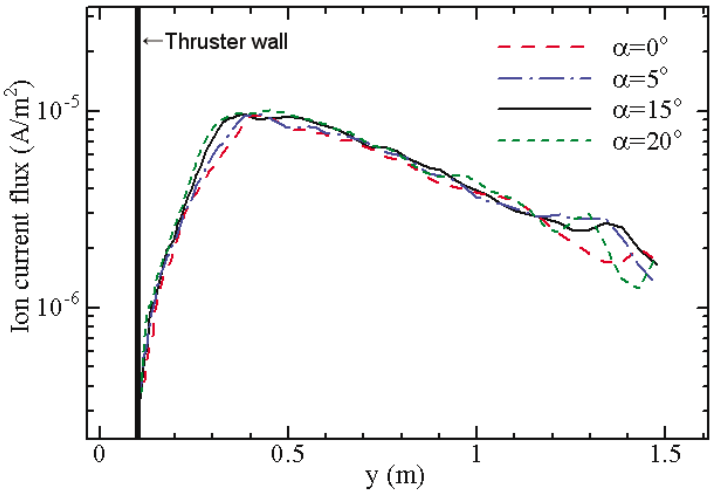

Figure 9. Sensitivity of radial profile of ion current flux to beam expansion angle α at x = -0.2 m. σ = $\sigma_{\rm cex}$, $G_{\rm p}$ = 0.6, α = 15°.

A radial profile of ion current flux at x = -0.2 m for various values of $\sigma_{\rm cex}$ are shown in Fig. 6. The calculations were made for $1\sigma_{\rm cex}$, $5\sigma_{\rm cex}$ and $10\sigma_{\rm cex}$. It can be seen that the ion current flux is increased with charge-exchange cross section and are strongly dependent on it. This result is reasonable because CEX ions are increased as the charge-exchange cross section increases.

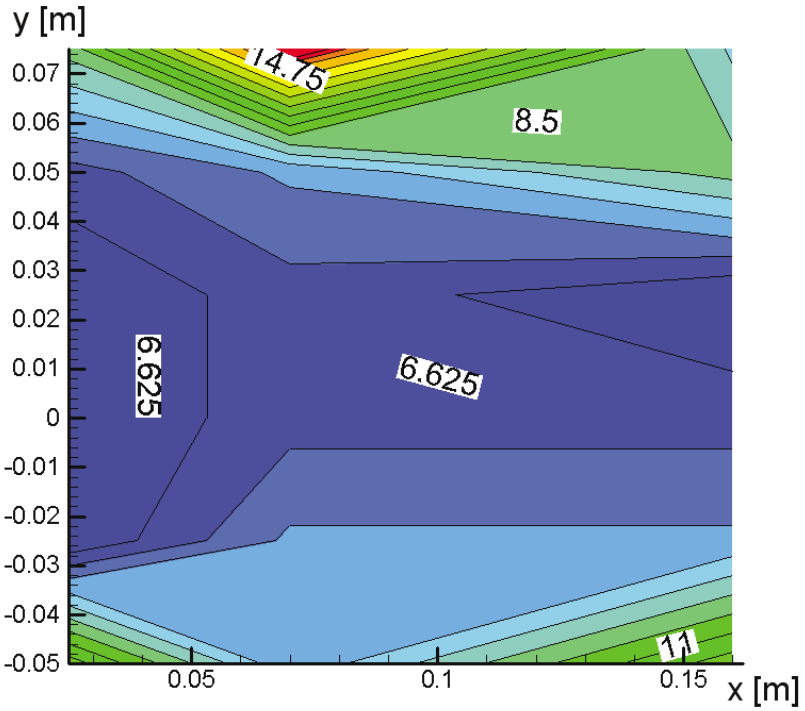

Figure 10. Contours of experimental electron temperature (unit in eV).

Sensitivity of a radial profile of ion current flux to electron temperature is shown in Fig. 7, where the electron temperature is assumed to be uniform in the entire flowfield. Electron temperature affects beam ions and ion velocities, and potential gradient is increased as $T_{\rm e}$ increases. Nevertheless, Fig. 7 shows very weak dependence of the ion current flux on electron temperature.

Figures 8 and 9 show radial profiles of ion current fluxes at x = -0.2 m for various values of $G_{\rm p}$ and α, respectively. The calculations were conducted for $G_{\rm p}$ = 0.1, 0.6 and 1.0, and α = 0°, 5°, 15°

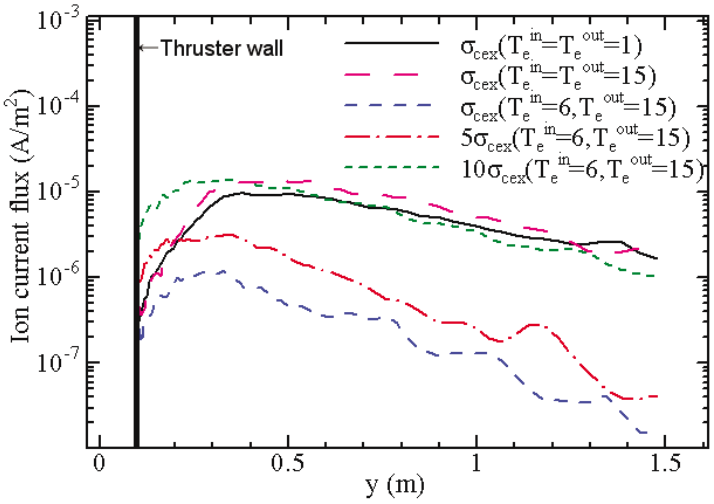

Figure 11. Radial profiles of ion current flux at x = -0.2 m for various values of $\sigma_{\rm cex}$. $T_{\rm e}^{\rm in}$ = 6 eV, $T_{\rm e}^{\rm out}$ = 15 eV

.

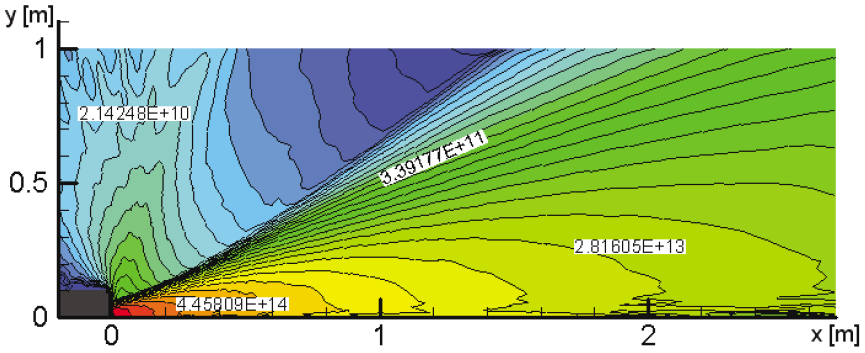

Figure 12. Contours of ion number density for uniform electron temperature. $T_{\rm e}^{\rm in} = T_{\rm e}^{\rm out}$ = 6 eV.

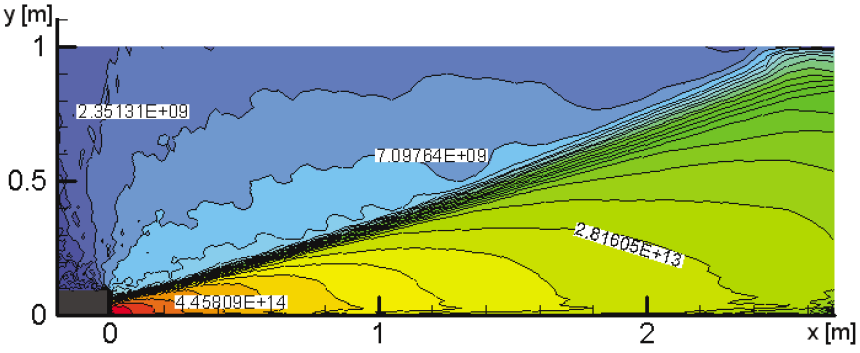

Figure 13. Contours of ion number density for non-uniform electron temperature. $T_{\rm e}^{\rm in}$ = 6 eV, $T_{\rm e}^{\rm out}$ = 15 eV.

and 20°. It may be mentioned that sensitivities of ion current flux to the Gaussian density profile coefficient ($G_{\rm p}$) and beam expansion angle (α) in the backflow region are negligibly small. In a real ion plume, electron temperature is considered not to be uniform in the entire flow field. Figure 10 shows experimental electron temperature in the plume from the MUSES-C ion engine. It can be seen that electron temperature is approximately 6 - 7 eV inside the beam and 10 - 15 eV outside it. In order to perform the simulation for the real flow field, it is assumed that electron temperature is 6 eV inside the beam and 15 eV outside it. Using this electron temperature distribution, the behavior of CEX ion in the backflow region was investigated for various values of charge-exchange cross section.

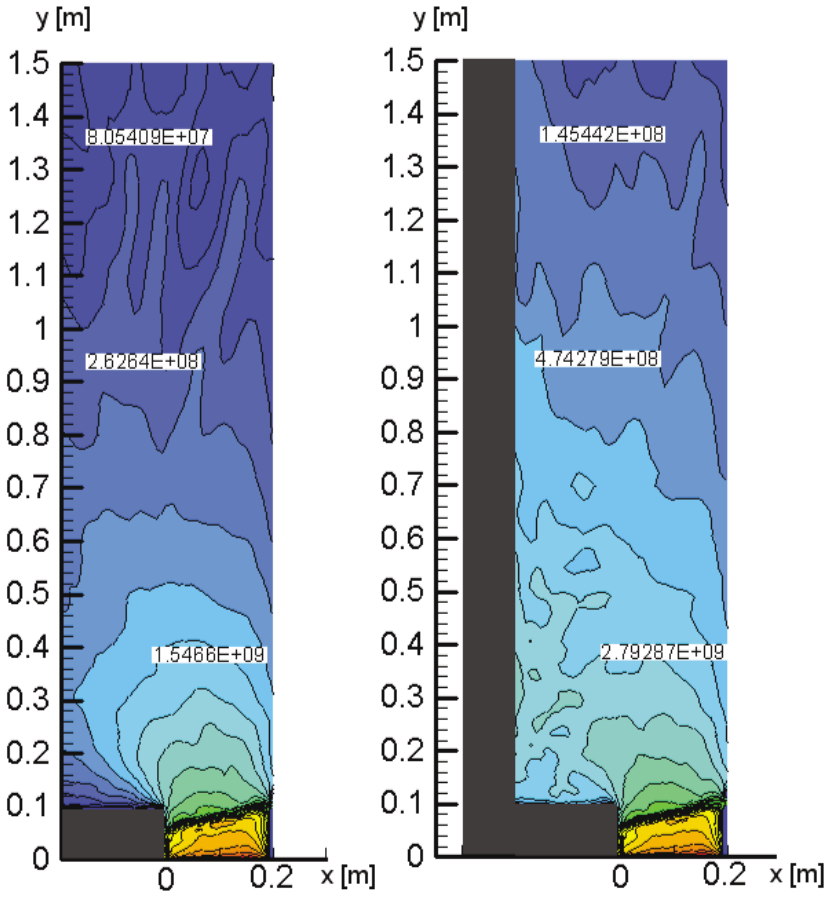

Figure 14. Contours of CEX ion number density (unit in m^{-3}).
left:without back wall, right:with back wall.

Radial profiles of ion current flux at x = -0.2 m for various values of σ_{cex} are shown in Fig. 11, where T_e^{in} and T_e^{out} are, respectively, the temperatures inside and outside the beam. In case of $1\sigma_{cex}$, the results for $T_e^{in} = T_e^{out} = 1$ eV and $T_e^{in} = T_e^{out} = 15$ eV are very close. This result is the same as already seen in Fig. 7. However, when in the latter case, the electron temperature inside the plume is changed to 6 eV and that outside is kept at 15 eV, the ion current flux is decreased by approximately an order of magnitude. Furthermore, the sensitivity to charge exchange cross section was investigated, taking $1\sigma_{cex}$, $5\sigma_{cex}$ and $10\sigma_{cex}$, and keeping at $T_e^{in} = 6$ eV and $T_e^{out} = 15$ eV. The results show an increase in the ion current flux with charge exchange cross section.

Contours of ion number density are illustrated in Fig. 12 for the uniform case that $T_e^{in} = T_e^{out} = 6$ eV, and in Fig. 13 for the non-uniform case that $T_e^{in} = 6$ eV and $T_e^{out} = 15$ eV. It can be understood from the comparison between Figs. 12 and 13 that the beam expansion is suppressed in the far downstream in case of $T_e^{in} = 6$ eV and $T_e^{out} = 15$ eV, which leads to smaller ion number density outside the beam.

As mentioned earlier, the potential gradient is increased with T_e. It has been understood from Fig. 11 that ion current fluxes for the non-uniform case of electron temperature are less than those in the uniform case. The main reason is presumably why higher electron temperature outside the beam gives higher outside potential than that inside the beam. Owing to this, CEX ions with small energy are closed inside the beam by the higher outside potential. It can be seen from a comparison between Figs. 12 and 13 that an ion beam is also affected by the potential.

3.3 Analysis of Backflow with Back Wall

Back wall like thruster wall or solar panel, etc. exists in the actual backflow region and CEX ions may interact with such back wall, so that computations were extended to the analysis of the backflow with wall. The back wall was placed at x = -0.2 m as shown in Fig. 2. In this section, $T_e^{in} = 6$ eV and

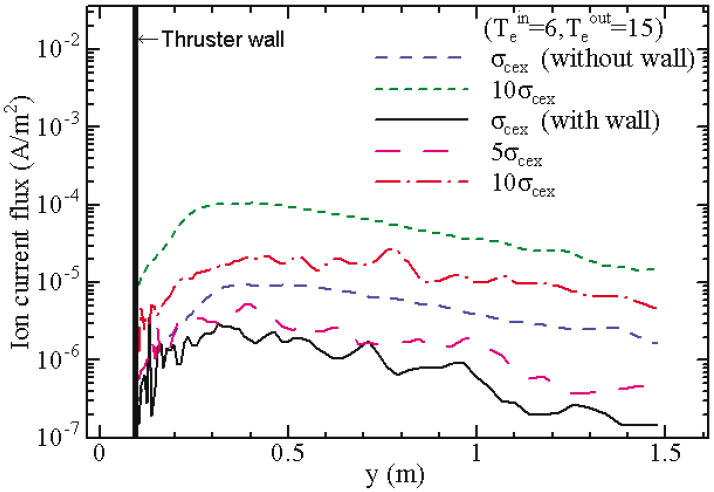

Figure 15. Effect of wall on ion current flux for $T_e^{in} = 6$eV, $T_e^{out} = 15$eV.

$T_e^{out} = 15$ eV were adopted, and diffuse reflection was imposed on the back wall. Calculations were made for three different values of charge-exchange cross section, i.e., $1\sigma_{cex}$, $5\sigma_{cex}$ and $10\sigma_{cex}$.

Contours of CEX ion number density in cases without and with back wall are shown in Fig. 14. In Fig. 15 radial profiles of ion current flux at x = -0.2 m for various values of σ_{cex} in case without back wall are compared with those in case with back wall. The result for case with back wall shows smaller ion current flux. This can be explained as follows: In case with back wall, the back wall prevents CEX ions from leaving the computational domain, which leads to larger number density of CEX ions in the back flow region as shown in Fig. 14. Larger number of CEX ions form a self-consistent electric field in the backflow region, and as a result CEX ions which reach the region are decelerated by them.

4 Conclusions

A plume from the MUSES-C ion engine was numerically analyzed using the DSMC-PIC method. Computed results were compared with experimental ones, and the optimal parameters were sought so as to fit to the experiments. Thus determined optimal parameters were the beam expansion angle of 15° and the Gaussian density profile coefficient of 0.6.

The behavior of CEX ion in the backflow region was investigated for various values of charge-exchange cross section, electron temperature, Gaussian density profile coefficient and beam expansion angle. One of these parameters was set as variable, and the other three parameters were fixed. The results showed that ion current fluxes were dependent on the charge-exchange cross section, but not on the other three parameters in the case of uniform electron temperature.

According to the experiments of the plume from the MUSES-C, electron temperatures inside and outside the beam were set to 6 eV and 15 eV, respectively. In case of non-uniform electron temperature, ion current fluxes were less than those in the uniform case. The main reason for this result is considered as follows: Higher electron temperature outside the beam, higher potential there. The higher potential shuts up CEX ions inside the beam.

Finally, the effect of the back wall on the behavior of CEX ions was investigated. In this case, the ion current flux was less than in case without back wall.

References

[1] G. A. Bird, *Molecular Gas Dynamics*, Clarendon Press, Oxford, England, 1976.

[2] G. A. Bird, *Molecular Gas Dynamics and the Direct Simulation of Gas Flows*, Clarendon Oxford, 1994.

[3] C. K. Birdsall and A. B. Langdon, *Plasma Physics Via Computer Simulation*, Adam Hilger, 1991.

[4] C. K. Birdsall and D. Fuss, Clouds-in-Clouds, Clouds-in Cells Physics for Many-Body Simulation, J. Comp. Phys., Vol.3, pp. 494–511 (1969).

[5] J. Wang and J. Brophy, 3-D Monte-Carlo Particle-in-Cell Simulations of Ion Thruster Plasma Interactions, AIAA Paper 95-2826, 1995.

[6] J. Wang, J. Brophy, and D. Brinza, 3-D Simulations of NSTAR Ion Thruster Plasma Environment, AIAA Paper 96-3202, 1996.

[7] R. I. Samanta Roy and D. E. Hasting, Three-Dimensional Modeling of Dual Ion-Thruster Plumes for Spacecraft Contamination, J. Spacecraft and Rockets, Vol.33, pp. 519–524 (1996).

[8] R. I. Samanta Roy, D. E. Hasting and N. A. Gatsonis, Ion-thruster Plume Modeling for Backflow Contamination, J. Spacecraft and Rockets, Vol.33, pp. 525–534 (1996).

[9] R. I. Samanta Roy, D. E. Hasting, and N. A. Gatsonis, Numerical Study of Spacecraft Contamination and Interactions by Ion-Thruster Effluents, J. Spacecraft and Rockets, Vol.33, pp.535–542 (1996).

[10] I. D. Boyd, D. B. VanGilder, and X. Liu, Monte Carlo Simulation of Neutral Xenon Flows of Electric Propulsion Devices, IEPC Paper 97-020, 1997.

[11] D. B. VanGilder, G. I. Font and I. D. Boyd, Hybrid Monte Carlo-Particle-in-Cell Simulation of an Ion Thruster Plume, J. Propulsion and Power, Vol.15, pp. 530–538 (1999).

[12] D. Rapp and W. E. Francis, Charge Exchange Between Gaseous Ions and Atoms, J. Chem. Phys., Vol.37, pp. 2631–2645 (1962).

[13] J. E. Pollard, Profiling the Beam of the T5 Ion Engine, IEPC Paper 97-019, 1997.

[14] J. Wang, J. Brophy, and D. Brinza, 3-D Simulations of NSTAR Ion Thruster Plasma Environment, AIAA Paper 96-3202, 1996.

[15] I. Funaki, H. Kuninaka, N. Onodera and S. Satori, Plasma Diagnostics of a Microwave Ion Engine, ISTS 98-a-2-20P, 1998.